PERGAMON

Journal of Structural Geology 26 (2004) 259–270

JOURNAL OF STRUCTURAL GEOLOGY

www.elsevier.com/locate/jsg

Experimental intracrystalline plastic flow in hot-pressed synthetic quartzite prepared from Brazilian quartz crystals

E.H. Rutter*, K.H. Brodie

Rock Deformation Laboratory, Department of Earth Sciences, University of Manchester, Manchester M13 9PL, UK

Received 15 August 2002

Abstract

Samples of synthetic, ultrafine-grained quartzite were prepared by hot-pressing aggregates of crushed, clear Brazilian quartz of mean grain size 0.4 μm at 300 MPa and 1373 and 1473 K. The samples displayed rapid grain-growth to ca. 12–20 μm with $<2\%$ porosity at 1473 K, facilitated by the 0.6 wt% of water adsorbed onto the grain boundaries during sample preparation. This water could be driven off by pre-heating, thereby preventing grain-growth. Sufficient water was incorporated during growth into the coarsened samples to render them weak and ductile. These were deformed experimentally in the β-quartz field using an argon gas medium apparatus at 300 MPa confining pressure at temperatures mainly between $T = 1273$ and 1473 K. Ductile flow was described by the flow law:

$$\dot{\epsilon} = 10^{-4.93}\sigma^{2.97}f(H_2O)\exp(-242000/RT)$$

with stress, σ, in MPa, and grain size, d, in microns and strain rate $\dot{\epsilon}$ in s^{-1}. R is the gas constant and $f(H_2O)$ is water fugacity. Based on observation of grain flattening, optical strain features, shapes and densities of dislocation arrays, and flow law parameters, samples deformed dominantly by dislocation creep, with some contribution from grain-boundary sliding.

Bearing in mind possible changes in the flow law parameters over the extrapolation interval and possible effects of the α–β phase transition, extrapolation to natural strain rates and temperatures predicts plastic flow at higher flow stresses at the same water fugacity at greenschist facies temperatures than previously published flow laws.

Keywords: Quartz; Plastic flow; Rock deformation

1. Introduction

From experimental work carried out over more than 30 years it has become clear that structure-bound water in quartz has a profound effect on its mechanical behaviour. 'Dry' single crystals of quartz, with a water content of less than 100 H/10^6Si, are strong and brittle, even at temperatures of 800 K and above (Griggs and Blacic, 1965; Hobbs et al., 1972; Blacic and Christie, 1984). In contrast, 'wet' single crystals, typically synthetic single crystals rapidly grown hydrothermally for the electronics industry, with total water contents of perhaps 4000 H/10^6Si, are weak and display intracrystalline plastic flow at temperatures of 800 K and above, even in the absence of confining pressure (Griggs and Blacic, 1965; Baëta and Ashbee, 1967; Hobbs et al., 1972; Linker and Kirby, 1981; Blacic and Christie, 1984).

The single crystal behaviour extends also to polycrystal behaviour. Even at high temperatures, at the low confining pressures (<500 MPa) typically associated with gas or other fluid media deformation machines, natural quartz polycrystals that are dry relative to synthetic crystals or rocks such as novaculite and flint, are strong and brittle. On the other hand, under the higher confining pressures typically associated with 'solid' medium deformation machines, not only is failure by fracture suppressed, so that differential stresses up to those commensurate with the theoretical strength can be applied, but many natural quartzites, bearing a wide range of water contents, can be deformed plastically to large strains and weakened further by addition of water prior to the experiment (den Brok et al., 1994). 'Natural' microstructures (intracrystalline optical

* Corresponding author. Tel.: +44-161-275-3947.
E-mail address: e.rutter@man.ac.uk (E.H. Rutter).

0191-8141/03/$ - see front matter © 2003 Elsevier Ltd. All rights reserved.
doi:10.1016/S0191-8141(03)00096-8

strain features and dynamic recrystallization) and large plastic strains can be produced (Kronenberg and Tullis, 1984; Koch et al., 1989; Hirth and Tullis, 1992; Gleason and Tullis, 1995; Post et al., 1996).

Through such solid media experimentation and refinements thereof, it has been possible to obtain constitutive laws to describe the intracrystalline plastic deformation of quartz under assumed 'steady state flow' conditions, and to investigate the different temperature/strain rate regimes of microstructural evolution and dynamic recrystallization (Hirth and Tullis, 1992). It has always been necessary experimentally to deform rock-forming minerals at 'unnaturally' high temperatures in order to shorten the timescale of deformation sufficiently for the process to be studied in the laboratory. Post et al. (1996) have demonstrated that there is a correlation of the weakening effect with water fugacity, which is enhanced by the high pressure conditions of experiments in solid media equipment. Potentially, it is the additional trade-off between water fugacity and strain rate that explains why quartzites deform plastically at natural strain rates, whilst 'unnaturally' high water fugacities are needed to do the same in the laboratory (Kohlstedt et al., 1995).

Paterson (1989) has pointed out how difficult it is to diffuse sufficient water into quartz under experimental conditions in gas confining media testing equipment at moderate pressures (e.g. 300 MPa). The result has been that weakness and enhanced plasticity has only been achieved at ca. 300 MPa confining pressure in very wet, synthetic quartz single crystals (e.g. Hobbs et al., 1972), in polycrystalline samples grown from wet, amorphous silica (Luan and Paterson, 1992) or in naturally wet aggregates such as flint (Mainprice, 1981). In this paper we demonstrate that it is possible to introduce water into naturally dry, Brazilian quartz by grain growth in a wet environment, and as a result to induce intracrystalline plastic flow of a quartz polycrystal in a gas medium apparatus at only 300 MPa confining pressure.

2. Sample preparation and characterization

The polycrystalline samples used in this study were prepared by hot isostatic pressing (HIP) of crushed single crystals of natural Brazilian quartz that were clear and free from optically-visible fluid inclusions. The selected crystals were crushed into fragments a few millimetres across and contaminated or opaque material was removed by hand picking. The remaining material was washed in hydrochloric acid and rinsed with distilled water before crushing in a TEMA tungsten carbide mill. The size fraction less than 64 μm was separated by sieving, so that the coarser material could be ground again. The fine fraction was separated into three sub-fractions by centrifuging in water, each with a modal grain size of 0.4 ± 0.15, 1.3 ± 0.4 and 4.0 ± 2.5 μm. The finest fraction was collected by settling from large volumes of water. All samples were finally dried in an oven at 90 °C and stored in glass bottles ready for hot isostatic pressing.

The water content of the starting crystals was determined by infra-red (IR) spectroscopy to be near the lower limit of detection, on the order of 10 to 20 H/10^6Si. This is a level of structure-bound water usually associated with high strength and brittleness in the experimental deformation of single quartz crystals (e.g. Hobbs et al., 1972). The amount of water adsorbed onto the surfaces of the grains in the three grain-size fractions to be used for hot pressing was measured by thermogravimetry (Fig. 1). Samples, 20 mg in size, were step heated to 1373 K in an open platinum sample holder in argon gas, whilst weight loss and differential thermal analysis were carried out. The finest size fraction showed a weight loss of about 0.6%, which corresponds approximately to one or two molecular layers of adsorbed water (about 1 nm thickness) on grains of mean size 0.4 μm. The specific surface area of the coarser samples is so much smaller than that of the finest sample material that an adsorbed layer would not be expected to produce (within an instrumental resolution of about 0.1 wt%) an unambiguous weight-loss signal on heating, and no clear weight loss was detected.

To investigate whether the quartz surfaces could be dried and kept dry, 1 g fractions of samples prepared as above were heated at 1373 K in air to drive off the adsorbed water, then held in a water-saturated atmosphere and weighed frequently over a 3 month period. No weight increase was detected that could correspond to resaturation of the surfaces with a monolayer or more of water. This lack of re-adsorption was confirmed by thermogravimetry, which showed no weight loss on re-heating to 1373 K. It has previously been found (Iler, 1979; P. Dove, personal comm., 1999) that pyrolysis of quartz leaves the surface hydrophobic, in contrast to the hydrophilic character of freshly cleaved surfaces (Parks, 1984).

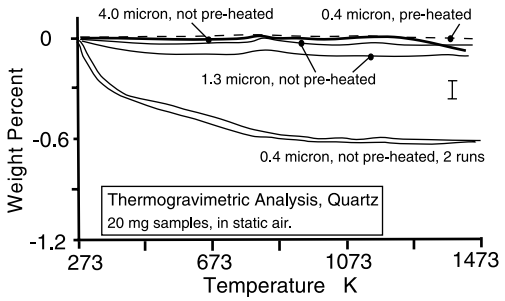

Fig. 1. Thermogravimetric analyses of nominally 20 mg samples of starting quartz powders, showing weight loss with progressive heating in an argon gas atmosphere. The initially 0.4 μm samples (as-ground) show a weight loss of ca. 0.6 wt%, corresponding to water adsorbed on the grain surfaces. The 1.3 μm samples showed a much smaller weight loss. The initially 4.0 μm samples and the 0.4 μm pre-heated (to 1373 K) samples showed no weight loss above the resolution of the instrument.

3. Experimental methods

3.1. Apparatus

All experiments were performed in a Paterson Instruments argon gas medium testing machine at 300 MPa confining pressure, at temperatures ranging between 1273 and 1473 K. At 300 MPa confining pressure the specimen is expected to be within the β-quartz stability field during compression experiments. Each specimen, nominally 1 cm in diameter and 2 cm long, was heated by a 3-zone furnace capable of maintaining temperature constant within better than 10 K along the length of the sample. Temperatures (at the thermocouple position at the top end of the sample) are expected to be correct within ± 7 K at 1473 K. Reported experiments include constant displacement rate, constant stress (creep) and stress relaxation tests.

Axial load was applied via a 100 kN servo-controlled electromechanical actuator. External load was measured using a 100 kN Instron load cell, which also provided the calibration standard for a capacitance-type internal load cell. Resolution of load measurement was about 50 N, but the smallest resolvable load on the sample was influenced greatly by the uncertainties in the load supported by the 0.35 mm wall thickness of iron jacket surrounding the specimen. Spot measurements of jacket strength were made using a copper dummy specimen at 1273 K and found to be reasonably consistent with jacket strengths calculated from the deformation mechanism map for iron (Frost and Ashby, 1982). The iron flow law was therefore used to extrapolate jacket strengths to 1473 K and also to lower temperatures. Thus at 1473 K, about 3 MPa of the apparent stress on a sample at 10^{-4} s^{-1} strain rate is expected to be supported by the jacket, or 5 MPa at 1273 K.

3.2. Specimen hot-pressing and grain growth

Samples of each of the initial grain sizes, both as-ground and subsequently dried by heating to 1373 K, were prepared for investigation of the hot-pressing behaviour by packing the powder into a short iron jacket, 45 mm long and 0.2 mm wall thickness. The powder was uniaxially cold-pressed in a thick-walled steel split-die to 300 MPa. This pressure is much too low to induce significant grain fracture at the grain sizes used (Zhang et al., 1990). Each specimen was weighed and measured to allow the starting porosity (typically $45 \pm 2\%$) to be determined. Iron discs of 0.1 mm thickness were placed at the ends of the cylindrical specimen to prevent reaction between the quartz and the recrystallized alumina loading pistons. The excess iron at the ends of the samples were machined off and the iron-sheathed specimen was loaded into the outer iron jacket, between the two loading pistons. The ends of the two loading pistons were capped off with 3-mm-thick recrystallized alumina discs to protect the piston ends and to prevent extrusion of the sample material up the hollow loading piston bearing the axial thermocouple.

The specimens were not weld-sealed inside their jacket assemblies. However, it is unlikely that any gas or other vapour pressure developed in the pores of the rocks would leak past the iron and alumina discs at each end of the specimen, provided such a pressure was always less than the confining pressure. Any such leakage would show as a pressure rise on the pore pressure gauge, and this was never seen to happen unless a perforation of the jacket occurred.

No measurements of the compaction of the specimen could be made during initial pressurization and heating, owing to the changes in the dimensions of the vessel and loading system with pressure and temperature. Isostatic compaction was first carried out at 300 MPa confining pressure at 1373 K for 24 h, then at 1473 K for a further 3 h, so that all specimens would be exposed to the most extreme temperature used in this series of tests. During hot-pressing at constant temperature, compaction could be measured by putting the machine into force-control mode with a nominal 1 MPa applied differential stress, so that a creep curve was obtained at near zero differential axial load. Virtually all of the recorded deformation was due to porosity reduction. It was found that the above compaction procedure reduced the compaction rate to a small residual value. The corresponding residual value of porosity could only be determined by microstructural analysis after the experiment.

Neither the samples fabricated from the two coarser size fractions, nor those prepared from the pre-dried 0.4 μm size fraction showed any grain growth during hot pressing. These samples were retained for a separate study of grain-size sensitive deformation of quartzite. Only the as-ground, initially 0.4 μm grain size samples, exhibited grain growth to ca. 12–20 μm uniformly equigranular grain size (Table 1). This grain size is sufficiently large to be seen in optical thin-sections (Fig. 2b). Scanning electron microscopy (SEM) of the samples revealed a very fine dispersion of tungsten carbide particles (on the order of 10 nm particle size, from the grinding) within quartz grain boundaries. It is inferred that these may have helped inhibit grain growth in all samples except the 0.4 μm as-ground samples that had a significant volume fraction of adsorbed grain-boundary water. Drying these samples in air at 1373 K prior to hot-pressing totally prevented grain coarsening.

The porosity and grain sizes of samples were determined after each experiment, but samples Q13a and Q15a were run under hydrostatic conditions only, to evaluate the role of compaction without deformation on grain growth (Table 1). These demonstrated that no grain growth occurred during heat treatment at 1373 K alone, but only after heat treatment at 1473 K, and that no further significant grain growth occurred during subsequent deformation. Final mean porosities of the hot-pressed and coarsened samples and deformed samples typically lay in the range 1–2% (Table 1). Thus, assuming isotropic compaction, specimen dimensions

Table 1
Summary of test conditions and results for each sample. Mechanical data for all samples are presented graphically in Figs. 4–6. Error values on grain size are standard deviation on the measured mean grain size. Confining pressure was 300 MPa

Sample nr.	Grain size (μm)/porosity %	Time at 1473 K (h)	Strain rate (s^{-1})	Flow stress (MPa)	Temp. (K)	Strain (%)	History
Q13a	13.7 ± 2.0	66.2	–	–	1473	–	Static heat treatment only.
	<1%						
Q15a	0.64 ± 0.05	71.8 at 1373 K	–	–	1373	–	Static heat treatment only at 1373 K.
	<1%						
Q7	18.7 ± 3.3	10.6	5.0×10^{-5}	167	1473	4.0	Const. strain rate + stress relaxation.
	1.7% ± 1.2		2.0×10^{-4}	238	1473	11.0	Const. strain rate + stress relaxation.
Q14	20.5 ± 1.0	4.5	3.8×10^{-5}	365	1373	5.0	Const. strain rate + stress relaxation.
	2.1% ± 0.7						
Q16	14.6 ± 1.1	4.8	4.0×10^{-5}	170	1473	2.0	Const. strain rate + stress relaxation.
			7.0×10^{-6}	160	1373	8.0	Const. strain rate + stress relaxation.
			2.0×10^{-5}	175	1473	13.0	Const. strain rate + stress relaxation.
Q18	16.0 ± 2.7	6.1	8.0×10^{-5}	350	1473	6.0	Const. strain rate.
	1.5% ± 0.5						
Q19	17.4 ± 1.3	29.8	4.0×10^{-5}	242	1473	5.0	Const. strain rate + stress relaxation.
Q20	–	21.8	4.0×10^{-5}	222	1473	10.0	Const. strain rate. Deformed specimen not recovered.
Q21	11.8 ± 7.7	32.1	7.0×10^{-5}	180	1473	6.0	Const. strain rate + stress relaxation.
	1.9% ± 0.7		1.3×10^{-5}	180	1373	9.0	Const. strain rate.
			1.0×10^{-5}	180	1373	11.0	Const. strain rate + stress relaxation.
			3.2×10^{-6}	190	1273	13.0	Const. strain rate + stress relaxation.
			3.2×10^{-6}	130	1473	18.0	Const. strain rate + stress relaxation.
Q30	12.2 ± 1.2	11.3	5.8×10^{-5}	222	1473	5.0	Const. strain rate + stress relaxation.
	2.7% ± 0.8		1.0×10^{-6}	85	1473	12.0	Const. strain rate.
			1.1×10^{-6}	66	1473	13.0	Const. stress.
			2.0×10^{-7}	66	1373	15.0	Const. stress.
			2.0×10^{-5}	422	1373	22.0	Const. strain rate + stress relaxation.

would typically change by 12–13%. Compacted samples retained a good cylindrical geometry.

As described below, these coarsened samples were weak and flowed plastically in the gas medium apparatus at 1473 K at differential stresses between 70 and 300 MPa at normal laboratory strain rates. Transmission electron microscopy (TEM) study of the coarsened samples (Fig. 2d) showed extensive formation of sub-micron vapour bubbles (such as turn quartz milky) and a rapid rate of structural damage to the samples under the electron beam (Kronenberg, 1994). These characteristics are typical of quartz with a large amount of structure-bound water. The 0.6 wt% of adsorbed water on the as-ground, 0.4 μm grain size fraction is more than enough water to weaken quartz if taken into the structure. It appears, therefore, that the migration of the grain boundaries that occurs during grain growth allows some of the intergranular water to be incorporated into the quartz. X-ray diffraction analysis of coarsened samples showed that they were almost 100% quartz, but small amounts (<1%) of cristobalite were also noted, despite the growth conditions being well outside the cristobalite stability field. This suggests the possibility that cristobalite may be involved kinetically in favouring the rapid grain growth.

It is of importance to estimate the amount of pore pressure that can be generated from the expansion of adsorbed water on the quartz grains, in order to evaluate the potential role of pore pressure in the mechanical behaviour and to estimate the water fugacity, $f(H_2O)$. Fig. 3 shows the rate of rise of pore pressure expected during compaction at 1373 K, assuming the measured 0.6 wt% water adsorbed on the 0.4 μm size fraction quartz and a typical final porosity of 1.25%, and neglecting competing processes that consume pore water (see below). The calculation assumes ideal-gas behaviour of water. This assumption is valid up to about 200 MPa pressure (Bowers, 1995), beyond which the curves slightly underestimate the pressure attained. This calculation predicts that an upper-bound pressure approaching 300 MPa pore pressure (equal to the confining pressure) might be produced during compaction.

Paterson (1989) estimated that diffusion of water into quartz would be significant at the scale of the initial grain sizes and at the temperatures used in these experiments. Some water is also consumed by dissociation and reaction with the iron jacket to produce oxide grains at and near the quartz-iron interface. In the case of the initially coarser (1.3 and 4.0 μm) samples, with less adsorbed water, the pore pressure produced is always expected to be substantially less than the confining pressure (Fig. 3), and it was clearly never enough to favour the accelerated grain growth that was seen in the 0.4 μm samples.

A point of concern is whether the presence of water in these sample assemblies is likely to have led to any significant melting at 1473 K, which might affect the flow behaviour. With system water contents >10%, quartz melts at 1373 K (Kennedy et al., 1962). When water is produced

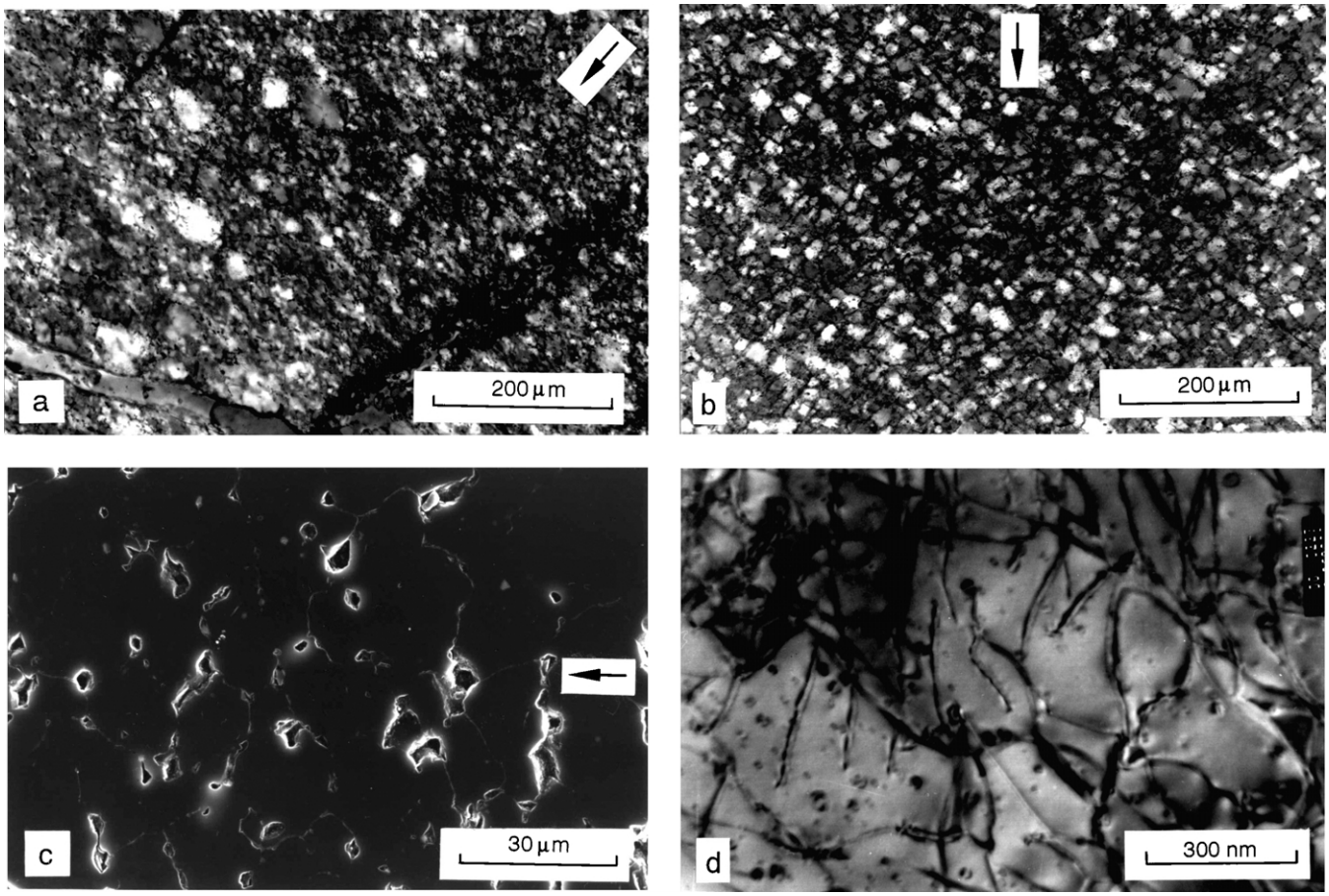

Fig. 2. Microstructures of experimentally deformed samples. In (a), (b) and (c) the maximum shortening direction is indicated by an arrow. (a) Optical micrograph of central portion of sample Q21, shortened about 33%, showing flattened grains (crossed polars with gypsum plate). (b) Optical micrograph of lower strain area in sample Q21 (crossed polars with gypsum plate). Grains are more nearly equant, but with boundaries aligned in high shear stress orientations, otherwise this area appears typical of one that has been coarsened but not deformed. (c) Secondary electron image of polished surface of sample Q7 near the loading piston where it is protected from the effects of deformation. It was coarsened to about 19 μm grain size at 1473 K prior to deformation. Traces of grain boundaries are just visible joining the pore spaces. Porosity at this point is about 5%, but varied from place to place between about 7 and 0.5% (average 1.7%). (d) Transmission electron image of the interior of a grain in the central part (most deformed) of sample Q7, showing well developed dislocation creep microstructure and a large density of water bubbles precipitated from the quartz structure.

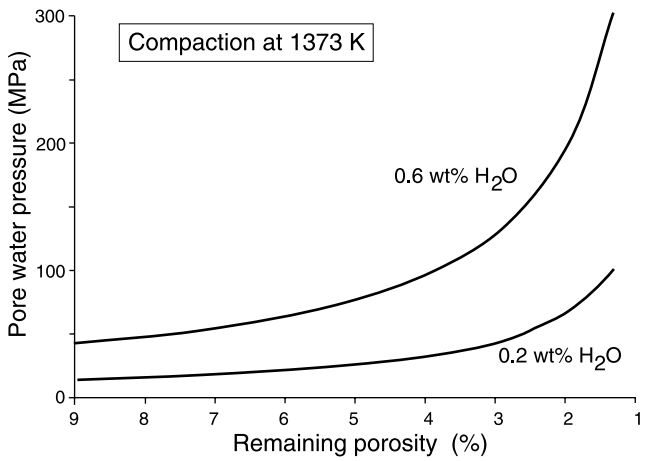

Fig. 3. Theoretical maximum elevation of pore water pressure with progressive compaction for an initial 0.6 and 0.2 wt% water in the pore spaces, neglecting water loss through dissolution in the quartz, and reaction with the iron jacket.

from the breakdown of a hydrous phase such as mica, local water contents may become high enough to promote some local melting. In these experiments, however, the total water content, which never exceeds 0.6 wt%, is always uniformly distributed. At water contents less than 3 wt%, melting is suppressed to temperatures greater than 1473 K. It is possible that a trace amount of melting on some grain surfaces may have occurred at 1473 K in some tests when porosity might have been reduced sufficiently to generate a transient substantial water pressure, but generally the consumption of water by (a) oxidation of the iron jacket and (b) by incorporation in the quartz by diffusion and grain boundary migration must prevent the attainment of the theoretical peak water pressure and suggests melting was unlikely. No microstructural features were seen that might indicate melting had occurred. Rapid grain growth seems to be arrested after a grain size of ca. 15–20 μm has been produced. This is inferred to be due to some combination of reduced driving force as grain size increases and through the

consumption of intergranular pore fluid by the above processes, leading ultimately to a low residual pore water pressure prior to deformation.

At 1373 K, between 1 and 300 MPa, the fugacity coefficient of water is very close to unity (Paterson, 1986), thus the curves shown in Fig. 3 are almost identical to the expected form of the variation of water fugacity during progressive compaction. Grain growth in a high (although not constant) water fugacity environment is likely to be responsible for the weakness and plasticity observed in the coarsened samples (Post et al., 1996). It cannot, however, be assumed that chemical equilibrium ever existed between the water fugacity in the vapour phase and in the quartz. As is observed in the fabrication of hydrothermal quartz crystals for the electronics industry, large and metastable supersaturations of water are incorporated into quartz during rapid growth, but much smaller amounts during slower growth (Lias et al., 1973).

We attempted to determine total water content of specimen Q19 after deformation using IR spectroscopy at room temperature. The integrated absorbance was about $\times 10$ greater than the starting single crystals, corresponding to ca. 100 to 200 H/10^6Si, although it is unclear what effects are introduced when attempting IR spectroscopy on a 200-μm-thick slice of polycrystal of grain size 15 μm.

3.3. Deformation experiments

All samples were initially loaded at a constant axial displacement rate that corresponded to strain rates in the range 10^{-7} to 10^{-3} s^{-1}. Most tests were punctuated or terminated by stress relaxation experiments (Rutter et al., 1978), in which the motor drive is stopped, and the stored elastic energy in the machine plus specimen is slowly dissipated by creep in the specimen, over a small increment of strain (typically 2%). Provided the machine plus specimen compliance is known, the stress relaxation behaviour can be recast as stress versus strain rate, which gives a rapid evaluation of rheologic response on a single test specimen. Strain rate stepping tests, in which the change in flow stress arising from a sudden change in deformation rate is observed, and stress-stepping in creep mode, were also used to help assess the stress sensitivity to strain rate behaviour.

Although most tests were run at constant temperatures of 1273, 1373 or 1473 K, a number of temperature stepping tests were performed in order to assess the strain rate sensitivity to temperature. Such tests can be used to determine the apparent activation enthalpy for flow, which is an essential parameter in the constitutive flow law and is required to extrapolate high temperature behaviour to low temperature, low strain-rate conditions.

No water was added to any of the specimen assemblies prior to testing. The only water in sample assemblies was that which was initially adsorbed onto the surfaces of the quartz grains.

In the experimental apparatus used, the specimen with its two loading pistons forms a laterally unsupported slender column, about 250 mm long where it passes through the furnace. Some experiments were therefore troubled by buckling or kinking instabilities in the specimen, which is detectable when the internal and external force gauge traces deviate from parallelism. This meant that several experiments could not be taken to strains exceeding about 16%. Inhomogeneous deformation above 15–20% shortening also means that mechanical data become progressively more unreliable at higher strains.

At the end of their deformation history, all specimens were rapidly offloaded and quenched at a rate determined by the thermal properties of the furnace. From 1473 K, samples would cool by 200 K in the first minute, and reach about 900 K by about 5 min later. Below this temperature any further microstructural adjustment is unlikely. During the quench, confining pressure dropped by about 50 MPa from 300 MPa.

Data processing involved correction of the measured actuator displacement for the amount of axial machine distortion, correction for the change in cross-sectional area of the specimen following hot-pressing and with strain (but assuming homogeneous deformation), and for the proportion of the load supported by the iron jacket. The first and third of these are affected by furnace temperature.

4. Experimental results

4.1. Mechanical data

Table 1 summarizes the experimental results for all of the samples tested that displayed grain coarsening, and Figs. 4 and 5 present the mechanical data in graphical form. In all tests the samples behaved wholly ductilely. There was never any localization of strain or any sign of brittle deformation, nor evidence for bulging of the specimen jacket, effects that would have arisen had pore pressures built up to a level greater than the confining pressure.

Fig. 4 shows stress–strain data for samples that had coarsened to ca. 12–20 μm grain size by hot pressing of initially 0.4 μm as-ground quartz powder, and Fig. 5 shows flow stress from constant displacement rate, constant stress and stress relaxation tests. Nearly all samples exhibited flow stresses equal to or less than the confining pressure, which suggests that any contribution to flow from dilatant fracturing and frictional processes is small. With a few exceptions, stress–strain curves display fairly sharp yield points and near-steady flow is quickly established. All specimens were deformed to more than 10% permanent strain, and specimen Q21 was taken to more than 30% bulk shortening. The scatter in flow stresses between different samples at the same temperature is tentatively attributed to variabilities between specimens in terms of microstructure and structure-bound water content.

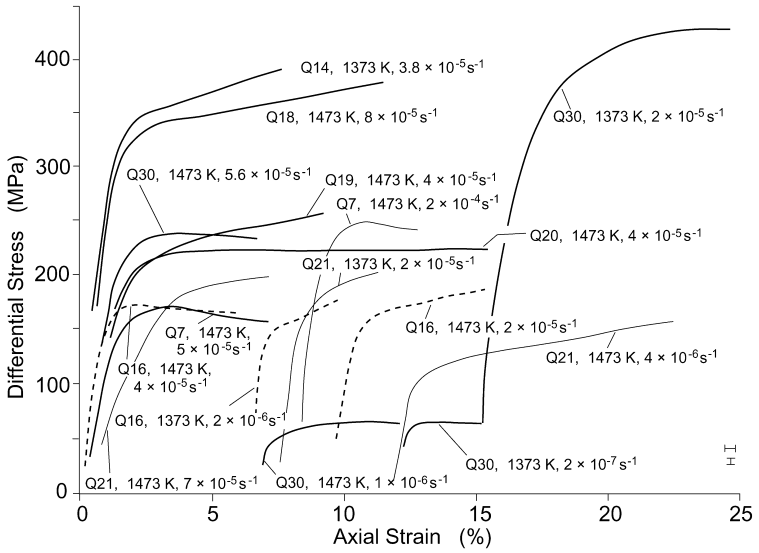

Fig. 4. Differential stress versus strain curves for coarsened samples fabricated by hot pressing initially 0.4 μm powder at 1473 K. Sample number, strain rate and temperature are indicated with each curve. Most tests were interrupted either by stress relaxations or by strain-rate stepping. Deformation of Q21 was continued to a nominal 33% shortening.

In Fig. 5 the 1473 K stress (σ MPa) versus strain rate ($\dot{\epsilon}$ s^{-1}) data extend over the largest range. A least squares fit to these data gave $\dot{\epsilon} \propto \sigma^n$, with $n = 2.97 \pm 0.29$ (1 standard error). Note that the large data content of the stress relaxation results dominate the position of the data centroid. There are fewer data at 1373 K but they too are consistent with this slope. The most reliable basis for activation enthalpy determination comes from temperature-stepping tests (Fig. 6), because specimen variability is not present in such tests. The mean of these determinations is 242 ± 24 kJ/mol. The best-fit lines shown on Fig. 5 therefore correspond to a flow law of the form $\dot{\epsilon} = A\sigma^n \exp(-H/RT)$ in which $n = 2.97 \pm 0.29$, $H = 242 \pm 24$ kJ/mol and $\log A = -2.45 \pm 0.39$, where stresses are

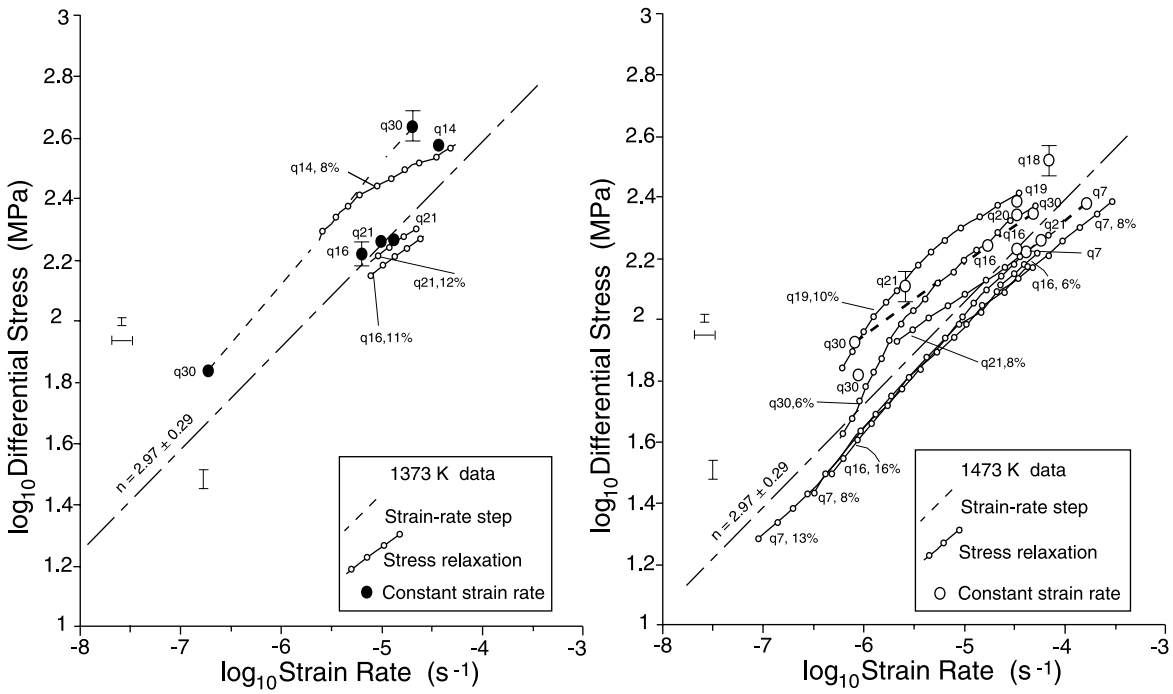

Fig. 5. Summary of mechanical data on coarsened samples at 1373 and 1473 K. Single points represent flow stress from stress–strain or creep data. Broken lines link data points in strain-rate stepping experiments. Error bars shown on particular points represent strain hardening behaviour, and show the range of flow stress from yield to the end of the period of deformation. General error bars indicate measurement uncertainty, and do not reflect variability between different specimens. Against stress relaxation curves are shown specimen number, strain at the centre of the stress relaxation range, and temperature. The long-dashed line on the 1473 K plot is a least-squares fit for that data to give best constraint on the slope $\partial \log \dot{\epsilon} / \partial \log \sigma = 2.97$. Using the activation enthalpy determined from temperature stepping tests (242 kJ/mol) to find the lateral offset, the long-dashed line on the 1373 K data has been plotted.

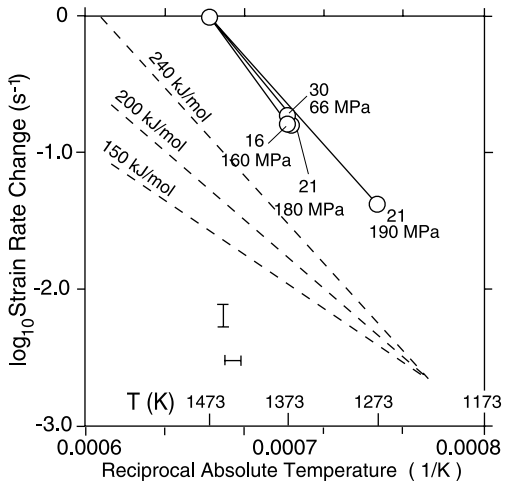

Fig. 6. Results of temperature stepping experiments performed to obtain the temperature sensitivity of strain rate. All temperature steps are referred to 1473 K. Beside points representing each temperature step is the specimen number and the differential stress at the temperature step. Uncertainty bars are shown for temperature and strain rate, and dashed lines show reference slopes corresponding to 240, 200 and 150 kJ/mol.

measured in MPa and strain rate in s^{-1}. Assuming the water fugacity in these experiments to have been 300 MPa, and writing the flow law in the form $\dot{\epsilon} = A\sigma^n f(H_2O)^m \exp(-H/RT)$, where m is taken to be one (following Hirth et al., 2001), the constant log$A$ becomes -4.93.

4.2. Microstructural observations

Samples were studied using optical microscopy, scanning electron microscopy (SEM) and high-voltage (300 kV) transmission electron microscopy (HVTEM) and by X-ray and electron backscatter texture analysis. Reported grain sizes (Table 1) and porosities were determined by the linear intercept method on typically more than 300 grains. Planar mean grain sizes are reported, with no stereological correction.

Starting microstructures: Fig. 2c shows the microstructure of the samples after heat treatment. The grain size is sufficient to allow examination using an optical petrographic microscope (Fig. 2b). The grain size is very uniform, except for a monogranular layer of larger grains (60 μm) nucleated directly on the iron jacket, and a narrow zone (about 0.5 mm wide) of less-coarsened material between the jacket and the coarsened central region of the specimen. Grain sizes (Table 1) were determined at the end of all experiments where an intact sample was recovered. Although the pre-deformation grain size could not be determined for each sample, observation of two coarsened but undeformed samples suggest that virtually all of the grain growth was complete before the start of each deformation experiment. No correlation between final grain size and total time at 1473 K was observed; neither was there any indication of a systematic relationship between final grain size and mechanical behaviour.

Deformed samples: It should be borne in mind that, because of stress and temperature stepping and stress relaxation cycles imposed on most samples, they have generally suffered complex deformation histories over a range of stresses, and that this might be expected to be reflected in their microstructural characteristics. Most specimens, however, were exposed to the lowest stresses of their histories at the point of offloading and quenching as a result of the last event being a stress relaxation, and microstructures are therefore most likely to be representative of this point.

Samples examined by TEM showed clear evidence of intracrystalline plasticity (Fig. 2d) in the form of a moderate density (3×10^9 cm^{-2}) of curved and non-coplanar dislocation lines, indicative of deformation involving dislocation glide and climb. A high density of small fluid bubbles (typically 20 nm diameter) also developed. This, together with very rapid observed rates of electron beam damage, is indicative of a high structure-bound water content in the quartz (Kronenberg, 1994). In contrast, the starting Brazilian quartz is very dry and free from dislocations. There was no evidence of mechanical interactions between dislocations and tungsten carbide particles (from powder grinding).

Crystallographic preferred orientation (CPO) analysis on three deformed samples (Fig. 7) revealed the development of crystallographic c-axis maxima (up to $\times 2$ uniform) about the compression direction plus a girdle normal to c, progressively strengthening with permanent strain. Quantitative analysis of grain shape in these samples also confirmed that grains became flattened by an amount corresponding to the imposed axial strain (Figs. 2a and 7). Experiment Q21 was terminated by a jacket failure whilst still under load, admitting gas to specimen pores and leading to brittle fracture by axial splitting (an axial crack is seen as a dark band in the lower right of Fig. 2a). Lower strain areas of specimen Q21 showed the development of rectangular grains, with the grain boundaries tending to align in orientations of high resolved shear stress (Fig. 2b). This observation suggests that, although deformation is dominated by intracrystalline plasticity, there may be a component of strain by grain-boundary sliding.

Gleason et al. (1993) showed that grain growth during deformation of flint and novaculite resulted in a c-maximum fabric parallel to compression in those grains that grew most rapidly under stress in a 'hard' orientation, to produce rhomb-shaped prophyroblasts. Thus the CPO observed reflected more the preferred growth than intracrystalline slip. We cannot discount a component of this effect in the crystallographic fabrics observed in the present study, but there are three factors that argue in favour of the fabric being at least partially due to intracrystalline slip. First, we observe that most grain growth occurs during the initial compaction, with little occurring during deformation,

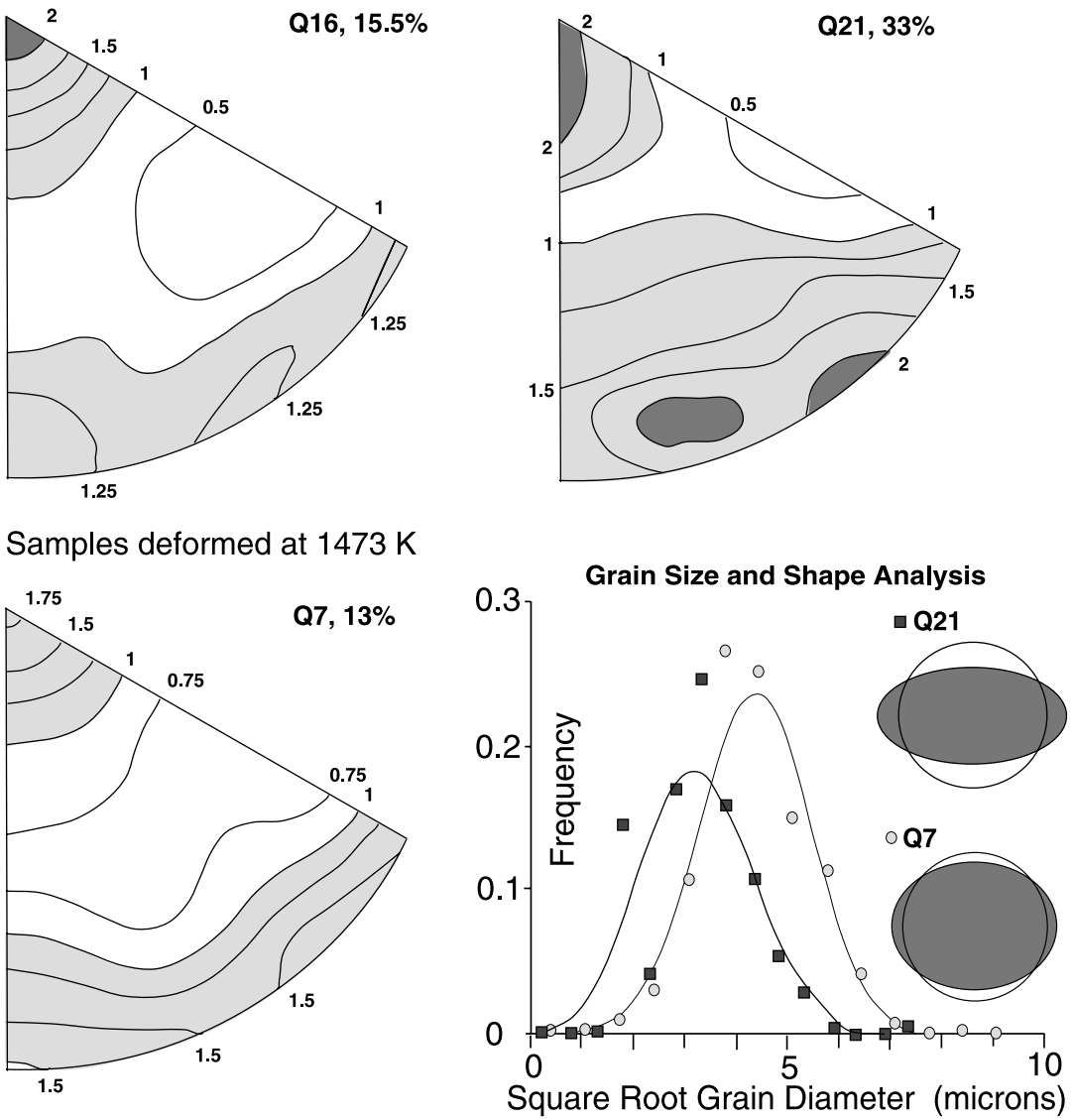

Fig. 7. Crystallographic preferred orientation (CPO) in experimentally deformed samples, shown as inverse pole figures contoured as multiples of uniform distribution. Specimen number, grain size and axial shortening strain are shown in each case. Lower right: grain size distribution and grain shape analyses for samples Q7 and Q21. The final grain shape (shaded ellipse relative to reference circle) reflects the bulk strain imposed. The Gaussian curves with the same mean and standard deviation as the data are shown for reference.

although we cannot discount some further selective growth of *c*-oriented grains during deformation. Second, the grain shapes in even the larger grains track the finite strain, suggesting they have not substantially changed size since the start of deformation, and they contain internal optical strain features such as subgrains. Third, the CPO is not simply a *c*-maximum fabric. There is also a significant development of *c*-axes normal to compression (Fig. 7), and there is some progressive intensification of the fabric with strain. It is possible that part of this total fabric is due to oriented growth and part to intracrystalline slip, but neither of the observed fabric components correlates with the small circle girdle of *c*-axes that Gleason et al. (1993) observed to be characteristic of intracrystalline plastic deformation and dynamic recrystallization of quartz under the conditions of their study.

5. Discussion and geological implications of results

5.1. Deformation mechanisms

The incorporation of water during grain growth from initially ultrafine aggregates is potentially a useful way to introduce water into quartz polycrystals for experimental purposes, whilst bearing in mind that metastably high concentrations may result of growth is rapid. In nature, slower growth may allow equilibrium to develop. The observation of uptake of water in this way also helps to underline the importance of grain boundary migration or neocrystallization of quartz during metamorphism as a mechanism for effective isotopic equilibration with the local pore fluid, as discussed by Kirschner et al. (1995) on the basis of evidence from the natural deformation and

recrystallization of Heavitree quartzite. This may be of particular importance in nature at low temperatures (300–350 °C), when diffusive re-equilibration in response to pore water pressure changes is likely to be too slow even on a geological time frame (Post and Tullis, 1998).

Deformation of these specimens with a stress exponent of 2.97, production of a grain flattening fabric, development of crystallographic preferred orientation through deformation (whilst bearing in mind the possible contribution of preferred growth to the observed fabrics), and development of uniform dislocation densities with typical recovery creep microstructures, are collectively indicative of flow by dislocation creep. Paterson (1989) and Paterson and Luan (1990) have drawn attention to the implications of n values less than 3.0 that have often been reported from experimental studies on plastic flow of quartzite. On theoretical grounds, a value between three and four should be expected for purely dislocation creep, and preferred for the extrapolation of experimental data to geological conditions, whereas a value smaller than three might be expected to arise from a contribution to strain from grain-boundary sliding, possibly assisted by the presence of melt. Only the experimental data reported by Luan and Paterson (1992), Gleason and Tullis (1995) and Post et al. (1996) yielded n values greater than three. The data of the present study are at the lower limit of the expected range of n and, as pointed out earlier, there is microstructural evidence that some grain boundary sliding may accompany intracrystalline plastic flow at the grain size of these samples. All of the above studies also reported lower values of activation enthalpy (H) for flow than obtained in this study. We were able to obtain several data over a temperature step from 1473 to 1373 K but only one measurement extending down to 1273 K. The extrapolation of experimental data to natural conditions is very sensitive to H, and the poor constraint on H must be regarded as a serious limitation to such extrapolation.

5.2. Extrapolation to geological conditions

Fig. 8 shows the result of extrapolating the flow law data for the plastically deformed, coarsened samples, to a 'natural' geological strain rate of 3×10^{-14} s^{-1}. The effect of the extrapolation of the estimated experimental errors is also shown. This extrapolation assumes that the flow law parameters determined for the experimental range do not change over the range of the extrapolation and that water fugacity remains constant at 300 MPa. It also ignores the effect of any changes in values of these parameters when crossing the α–β quartz transition. Linker and Kirby (1981) studied the effect of the α–β transition on the creep of hydrolytically-weakened single crystals of quartz in different crystallographic directions. Although there was a small increase in activation enthalpy for creep that varied according to loading direction with respect to crystallographic axes, and significant creep rate anisotropy, there was no large, stepwise jump in creep rate across the

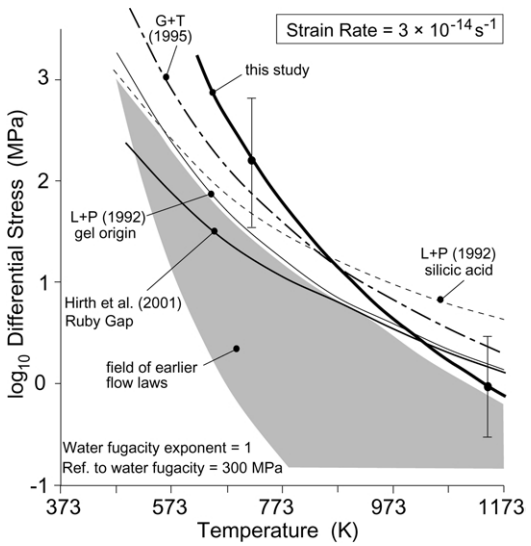

Fig. 8. Extrapolations of experimental data to a geological strain rate of 3×10^{-14} s^{-1}, all referred to a constant water fugacity of 300 MPa. The curves correspond to an intracrystalline plastic flow law of the form $\dot{\epsilon} = A\sigma^n f(H_2O)\exp(-H/RT)$. For that labelled 'this study' $n = 2.97 \pm 0.29$, $H = 242 \pm 24$ kJ/mol and $\log A = -4.93 \pm 0.34$, obtained for the samples coarsened from 0.4 μm at 1473 K (stresses in MPa). Uncertainty bars are for one standard deviation in experimental data after extrapolation, and similar levels of uncertainty apply to previously published extrapolations. Extrapolations of the plastic flow laws of Gleason and Tullis (G + T, 1995), Luan and Paterson (L + P, 1992) and Hirth et al. (2001) are also shown for comparison. These and the present study form an upper bound to the region occupied by pre-1992 flow laws for plastic flow of quartz (grey area, summarized in Rutter and Brodie (1992)).

boundary. Thus, although extrapolation of β-quartz polycrystal flow data across the α–β transition must introduce an error, it seems unlikely to be more important than uncertainties in the measured flow law parameters or concerning natural or metastable variabilities in water content.

Fig. 8 also shows corresponding extrapolations of the flow laws of Luan and Paterson (1992) and Gleason and Tullis (1995), together with the range of extrapolations using earlier flow laws that were summarized in Rutter and Brodie (1992). Also included, and referred to the same constant value of water fugacity (300 MPa), is the flow law of Hirth et al. (2001), who attempted to include additional constraints using combinations of strain rates and paleostresses inferred from observations of naturally deformed quartzite. These post-1992 flow laws, which are characterized by higher n values, predict strengths for quartz rocks at the upper bound of the bundle of extrapolations from earlier data. These higher predicted strengths for quartz rocks in nature are more satisfactory than earlier extrapolations, which have tended to predict that quartz rocks might be weaker than calcite rocks in nature, which would be in conflict with most geological field observations.

The curves shown in Fig. 8 would rise more steeply at lower temperatures if water fugacity were allowed to fall to lower values at lower temperatures, as it would with

decreasing depth in the Earth. Reducing water fugacity from 300 to 30 MPa would be expected to produce approximately a 2- to 3-fold strengthening.

Although there is a tendency towards convergence of flow law data for plastic flow of quartz rocks, there remains some considerable variability between the results of the different studies. The differences between the different extrapolations are commensurate with the level of uncertainty that would be associated with any one of them. These variations might be due to (a) extrapolation of different datasets some of which have to cross the $\alpha-\beta$ polymorphic transition, (b) differences in initial microstructure of the deformed samples, in the amounts of melt that may possibly have been present, and in the relative amounts of minor grain boundary sliding or brittle processes contributing to the flow, (c) differences in the degree of water incorporation into the sample materials in different studies, according to the methods of fabrication and treatment of samples. Large and metastable quantities of water can evidently be incorporated into quartz crystals, and even in experiments designed to control the intracrystalline water activity by buffering (Post et al., 1996) it remains unclear whether or to what extent equilibration has been achieved. If, in all of these experimental studies to date (including the present one), unnaturally large amounts of water have been incorporated, the flow law predictions of flow stresses at natural strain rates might best be regarded as giving lower bounds.

6. Conclusions

Synthetic, hot-pressed aggregates of ultrafine grained quartz, of mean grain-size 0.4 μm, prepared from crushed single crystals of Brazilian quartz, were found to undergo rapid grain growth to about 12–20 μm at 1473 K and 300 MPa confining pressure in a few hours. The grain growth was facilitated by a monolayer of adsorbed water on the grain surfaces. This water was taken into the quartz structure from the shrinking pore volume during grain-growth, leading to a lowering of the resistance to deformation by intracrystalline plasticity. Large plastic strains could be induced at low flow stresses, with development of a grain-shape fabric that reflected the bulk strain on the aggregate, and development of a crystallographic preferred orientation that was strengthened by increasing strain. An empirical power-law description of the flow was obtained, with a stress exponent (n) of 2.97, an activation enthalpy (H) for flow of 242 kJ/mol and a pre-exponential constant (A) of $10^{-4.93}$ MPa^{-n} s^{-1}, the latter term assuming strain rate varies linearly with water fugacity.

Bearing in mind the limitations of doing so, extrapolation of the experimentally observed intracrystalline plastic flow behaviour to low temperatures (<600 K) at 'natural' strain rates predicts flow stresses higher than those predicted for quartz aggregates from previous studies, but about the same at higher temperatures (e.g. 15 MPa at 873 K at a strain rate of 3×10^{-14} s^{-1}). The present experiments underline the role of structure-bound water in the facilitation of plastic flow in quartz, and the likely difficulty of controlling reliably the fugacity of water in quartz during deformation experiments.

Acknowledgements

This work was supported by UK NERC grant GR3/8627. Experimental Officer Robert Holloway helped maintain the experimental apparatus used in this study. Peter Morris is thanked for carrying out the IR analyses, Martin Casey and Walid ben Ismail, respectively, performed two X-ray and one electron backscatter texture determinations for us. Helpful and constructive comments from reviewers Jan Tullis and Greg Hirth are greatly appreciated.

References

Baëta, R.D., Ashbee, K.H.G., 1967. Plastic deformation and fracture of quartz at atmospheric pressure. Philosophical Magazine 15, 931–938.

Blacic, J.D., Christie, J.M., 1984. Plasticity and hydrolytic weakening of quartz single crystals. Journal of Geophysical Research 89, 4223–4239.

Bowers, T.S., 1995. Pressure–volume–temperature properties of H_2O–CO_2 fluids. In: Ahrens, T.H. (Ed.), Rock Physics and Phase Relations, A Handbook of Physical Constants. AGU Reference Shelf 3, pp. 45–72.

den Brok, B., Meinecke, J., Röller, K., 1994. Fourier transform IR-determination of intragranular water content in quartzites experimentally deformed with and without added water in the ductile deformation field. Journal of Geophysical Research 99, 19821–19828.

Frost, H.J., Ashby, M.F., 1982. Pure iron and ferrous alloys. In: Deformation Mechanism Maps, the Plasticity and Creep of Metals and Ceramics. Pergamon, New York, pp. 61–66.

Gleason, G.C., Tullis, J., 1995. A flow law for dislocation creep of quartz aggregates determined with the molten salt cell. Tectonophysics 247, 1–23.

Gleason, G.C., Tullis, J., Heidelbach, F., 1993. The role of dynamic recrystallization in the development of lattice preferred orientations in experimentally deformed quartz aggregates. Journal of Structural Geology 15, 1145–1168.

Griggs, D.T., Blacic, J.D., 1965. Quartz: anomalous weakness of synthetic crystals. Science 147, 292–295.

Hirth, G., Tullis, J., 1992. Dislocation creep regimes in quartz aggregates. Journal of Structural Geology 14, 145–159.

Hirth, G., Teyssier, C., Dunlap, J.W., 2001. An evaluation of quartzite flow laws based on comparisons between experimentally and naturally deformed rocks. International Journal of Earth Sciences 90, 77–87.

Hobbs, B.E., McLaren, A.C., Paterson, M.S., 1972. Plasticity of single crystals of synthetic quartz. In: Heard, H.C., Borg, I.Y., Carter N.L., Raleigh, C.B. (Eds.), Flow and Fracture of Rocks. American Geophysical Union Monograph 16, pp. 29–53.

Iler, R., 1979. The Chemistry of Silica, John Wiley and Sons, New York, 865pp.

Kennedy, G.C., Wasserberg, G.J., Heard, H.C., Newton, R.C., 1962. The upper three-phase region in the system SiO_2–H_2O. American Journal of Science 260, 502–521.

Kirschner, D.L., Teyssier, C., Gregory, R.T., Sharp, Z.D., 1995. Effect of deformation on oxygen isotope exchange in Heavitree quartzite, Ruby

Gap duplex, central Australia. Journal of Structural Geology 17, 1407–1423.

Koch, P.S., Christie, J.M., Ord, A., George, Jr., R.P., 1989. Effect of water on the rheology of experimentally deformed quartzite. Journal of Geophysical Research 94, 13975–13996.

Kohlstedt, D.L., Evans, B., Mackwell, S.J., 1995. Strength of the lithosphere: constraints imposed by laboratory experiments. Journal of Geophysical Research 100, 17587–17602.

Kronenberg, A.K., 1994. Hydrogen speciation and chemical weakening of quartz. In: Ribbe, P.H. (Ed.), Silica, Physical Behavior, Geochemistry and Materials Applications. Reviews in Mineralogy, Mineralogical Society of America 29, pp. 123–176.

Kronenberg, A.K., Tullis, J., 1984. Flow strengths of quartz aggregates: grain-size and pressure effects due to hydrolytic weakening. Journal of Geophysical Research 89, 4281–4297.

Lias, N.C., Grudenski, E.E., Kolb, E.D., Laudise, R.A., 1973. The growth of high acoustic Q quartz at high growth rates. Journal of Crystal Growth 18, 1–6.

Linker, M.F., Kirby, S.H., 1981. Anisotropy in the rheology of hydrolytically weakened synthetic quartz crystals, In: Carter, N.L., Friedman, M., Logan, J.M., Stearns, D.W. (Eds.), Mechanical Behavior of Crustal Rocks. American Geophysical Union Monograph 24, pp. 29–48.

Luan, F.C., Paterson, M.S., 1992. Preparation and deformation of synthetic aggregates of quartz. Journal of Geophysical Research 97, 301–320.

Mainprice, D.H., 1981. The experimental deformation of quartz polycrystals. Ph.D thesis. Australian National University, Canberra, 171pp.

Parks, G.A., 1984. Surface and interfacial free energies of quartz. Journal of Geophysical Research 89, 3997–4008.

Paterson, M.S., 1986. The thermodynamics of water in quartz. Physics and Chemistry of Minerals 13, 245–255.

Paterson, M.S., 1989. The interaction of water with quartz and its influence in dislocation flow—an overview. In: Karato, S.I., Toriumi, M. (Eds.), Rheology of Solids and of the Earth, Oxford University Press, Oxford, pp. 107–142.

Paterson, M.S., Luan, F.C., 1990. Quartzite rheology under geological conditions. In: Knipe, R.J., Rutter, E.H. (Eds.), Deformation Mechanisms, Rheology and Tectonics. Geological Society Special Publication 54, pp. 299–307.

Post, A.D., Tullis, J., 1998. The rate of water penetration in experimentally deformed quartzite: implications for hydrolytic weakening. Tectonophysics 295, 117–137.

Post, A.D., Tullis, J., Yund, R.A., 1996. Effects of chemical environment on dislocation creep of quartzite. Journal of Geophysical Research 101, 22143–22156.

Rutter, E.H., Brodie, K.H., 1992. The rheology of the lower continental crust. In: Fountain, D., Arculus, R., Kay, R. (Eds.), Continental Lower Crust, Elsevier Series on Developments in Geodynamics, pp. 201–268.

Rutter, E.H., Atkinson, B.K., Mainprice, D.H., 1978. On the use of the stress relaxation testing method in studies of the mechanical behaviour of geological materials. Geophysical Journal of the Royal Astronomical Society 55, 155–170.

Zhang, J., Wong, T-F., Davis, D.M., 1990. Micromechanics of pressure-induced grain crushing in porous rocks. Journal of Geophysical Research 95, 341–352.